Orthogonality Sampling for Object Visualization

Roland Potthast *

October 31, 2007

Abstract

The goal of this paper is to propose a new sampling algorithm denoted as *orthogonality sampling* for the detection of the location and shape of objects from the far field pattern of scattered waves. We will describe and analyse the method both for the reconstruction of an unknown number of small scatterers as well as for the classical shape reconstruction problem in acoustics. The basic and new feature of the algorithm is its *flexibility* and *stability* with respect to data settings and data error.

The basic idea of the method is to sample the space under consideration by calculating scalar products of the measured far field pattern $u^\infty(\hat{x})$, $\hat{x} \in \mathbb{S}$ with a test function $e^{i\kappa\hat{x}\cdot y}$ for all y in a subset Q of the space $\mathbb{R}^m$, $m = 2, 3$. The methods can reconstruct the location and shape of objects from measurements of the scattered field for *one* or *several* directions of incidence and *one* or *many* frequencies or wave numbers, respectively. We prove that the method reconstructs the *reduced scattered field* from the far field pattern and investigate the stability of the reconstructions. We will also provide a numerical proof of concept which shows that the method works well for a number of different situations and settings.

1 Introduction

Inverse scattering problems are of importance for many applications, for example for medical imaging, nondestructive testing, remote exploration, geophysical prospecting or radar. Usually, a wave is sent into a region of space which is to be investigated. Then, due to the structure of the unknown area or the existence of obstacles a scattered wave is generated which is measured far away from the objects under consideration. The task of *inverse scattering theory* is to reconstruct properties of the unknown scatterers from these remote measurements. Inverse scattering has developed into an important part of applied mathematics with a growing number of interesting and promising new mathematical techniques.

*Department of Mathematics, University of Reading, Whiteknights, PO Box 220, Berkshire, RG6 6AX, UK, r.w.e.potthast@reading.ac.uk

Inverse scattering theory has a long history with classical contributions for example by Lax and Phillips [8]. An introduction into the theory of acoustic and electromagnetic inverse scattering can be found in the work of Colton and Kress [3]. More recently, new classes of methods have been introduced with sampling and probe methods, see [1], [5], [9], [10]. Their main idea is to formulate an indicator function μ defined either in the space $\mathbb{R}^m$ or on a set of test domains. This function characterizes the unknown scatterers, their physical properties or their shape. Here, we will base our method on the evaluation of the scalar product

$$\mu(\tilde{y}) := |\int_{\mathbb{S}} e^{i\kappa\hat{x}\cdot\tilde{y}} u^\infty(\hat{x}) ds(\hat{x})|, \quad \tilde{y} \in \mathbb{R}^m \tag{1}$$

with $m = 2, 3$ and the unit sphere $\mathbb{S}$ in two or three dimensions, respectively. The functional (1) tests the *orthogonality relation* between the exponential and the far field pattern, from which the name *orthogonality sampling* is derived.

Let us briefly describe the orthogonality sampling idea in comparison to a range of well-established sampling and probe methods. Important sampling schemes have been introduced by Colton and Kirsch with the *linear sampling method* [1], by Kirsch with the *factorization method* [5], Ikehata and the author with the *probe method* or the *singular sources method* [10] (which have been shown to be equivalent) and by Luke and the author with the *no reponse test* [9]. Other schemes have been suggested by Sylvester, Kusiak and the author with the *range test* or by Ikehata with the *enclosure method*, compare the survey [9]. Each of these methods exploits different properties of the scattering map or particular scattered fields which are then reconstructed from the measurements.

First, all of the above methods have been introduced in the case of a fixed frequency or wave number, respectively. The methods of Colton-Kirsch and of Kirsch are based on the far field operator

$$(Fg)(\hat{x}) := \int_{\mathbb{S}} u^\infty(\hat{x}, \theta) g(\theta) ds(\theta), \quad \hat{x} \in \mathbb{S} \tag{2}$$

where $u^\infty(\hat{x}, \theta)$ denotes the far field pattern for scattering of a plane wave $u^i(y, \theta) := e^{i\kappa y\cdot\theta}$ with $y \in \mathbb{R}^m$ and $\theta \in \mathbb{S}$, where $m = 2, 3$ and $\mathbb{S}$ denotes the unit sphere in two or three dimensions, respectively. This means that these methods generically need to know measurements of the far field pattern at least on an open subset of the unit sphere for many incident plane waves (or more general for many linearly independent incident fields). The same setup is the basis for the probe method and the singular sources method of Ikehata and the author. We remark that the knowledge of the far field pattern of a time-harmonic wave for many directions of incidence builds a complete set of data in the sense that for any given incident field we can construct the far field pattern from the above measured data.

The *no response test*, the *range test* and the *enclosure method* need less data for reconstruction. These methods can be formulated based on the knowledge of the far field pattern for scattering of one incident time-harmonic wave only. This situation is

of particular interest for applications, since often it is not possible to measure for many incident waves with different directions of incidence. We remark that the geometrical setup for these methods is considerably more involved than for the linear sampling method or factorization method, since the indicator function is defined on a set of test domains, not directly in the real space. The methods employ *domain sampling*, not *point sampling*. The orthogonality sampling method proposed in this work will work for one direction of incidence, but employ a point-sampling principle.

Often, in applications measurements are taken in the time-domain, i.e. a time-dependent pulse is generated for which the time-dependent far field pattern is recorded. Via the Fourier transform it is then possible to extract the measured time-harmonic far field pattern for all frequencies which are part of the pulse. Here we will assume that a pulse contains the frequencies in an interval $[\kappa_0, \kappa_1] \subset \mathbb{R}^+$. Orthogonality sampling will be formulated for the case where the far field pattern is given for either one fixed frequency or for the *multi-frequency* case where the far field pattern is known for all wave numbers $\kappa \in [\kappa_0, \kappa_1]$. We will also demonstrate results for the fixed frequency case where the far field pattern is measured for several incident plane waves, which we refer to as *multi-direction* data.

In Section 2 we will introduce the basic notation and background for the analysis. We also describe the method which has been used to generate the forward data for the numerical reconstructions. In Section 3 we introduce the one-wave mono-frequency version of the orthogonality sampling. Here, we show that the method basically reconstructs a *reduced scattered field* based on a superposition of Bessel functions. We provide a proof via integral equation methods. We also provide some stability analysis for the reconstruction of the reduced scattered field. Section 4 introduces a *multi-frequency version* of the method. Section 5 introduces a version of the method for *multiple directions* and for the full multi-direction multi-frequency case. Finally, we provide a numerical study of the new scheme which proves the feasibility and stability of the method. In particular, we will show reconstructions both of an unknown number of scatterers and for the shape of some single scatterer.

2 The forward problem for multiple objects

The goal of this section is to define and solve the forward problem for scattering of a time-harmonic incident wave or of a time-dependent pulse by some obstacle. Here, for simplicity we will restrict our attention to the case of the Dirichlet boundary condition.

We consider the scattering of some *time-harmonic acoustic wave* u^i by an impenetrable scatterer D with *Dirichlet (sound-soft) boundary condition* in two or three dimensions. The scattered field is denoted by u^s and the total field $u = u^i + u^s$ is a solution to the *Helmholtz equation*

$$\triangle u + \kappa^2 u = 0 \tag{3}$$

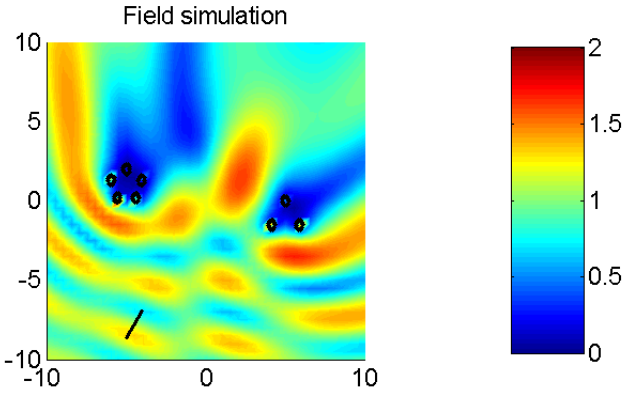

Figure 1: Total field $u = u^i + u^s$ for scattering of a plane wave with wave number $\kappa = 1$ and direction of incidence $\theta = (\cos(\pi/3), \sin(\pi/3))$. Here the scatterer consists of eight objects which are clustered in two groups.

in $\mathbb{R}^m \setminus \overline{D}$ with $m = 2$ or $m = 3$, where κ denotes the wave number. The scattered field is assumed to satisfy the *Sommerfeld radiation condition*

$$r^{\frac{m-1}{2}} \left(\frac{\partial u^s}{\partial r} - i\kappa u^s \right) \to 0, \quad r = |x| \to \infty, \tag{4}$$

uniformly in all directions $\hat{x} = x/|x|$. Further, we assume that the total field u satisfies the *Dirichlet boundary condition*

$$u = 0 \quad \text{on } \partial D. \tag{5}$$

It is well known (c.f. [3]) that a radiating scattered field u^s has the asymptotic behavior

$$u^s(x) = \frac{e^{i\kappa|x|}}{|x|^{\frac{m-1}{2}}} \left\{ u^\infty(\hat{x}) + O\left(\frac{1}{|x|} \right) \right\}, |x| \to \infty, \tag{6}$$

where u^∞ is the *far field pattern* of u^s. By $\mathbb{S}$ we denote the boundary of the unit disk or unit ball, respectively. The incident plane wave $u^i(x, d) := e^{i\kappa x \cdot d}$ for $d \in \mathbb{S}$ induces a scattered field $u^s(\cdot, d)$ with far field pattern by $u^\infty(\cdot, d)$. If the incident field is given by a point source

$$\Phi(x, y) = \begin{cases} \dfrac{i}{4} H_0^{(1)}(\kappa|x - y|), & m = 2, \\ \dfrac{1}{4\pi} \dfrac{e^{i\kappa|x-y|}}{|x - y|}, & m = 3, \end{cases}$$

with the Hankel function of the first kind and order zero $H_0^{(1)}$, we denote the scattered field by $\Phi^s(\cdot, y)$ and its far field pattern by $\Phi^\infty(\cdot, y)$, $y \in \mathbb{R}^m \setminus \overline{D}$.

For every domain G with $D \subset G$ we have *Green's formula*

$$u^s(x) = \int_{\partial G} \left(\Phi(x,y) \frac{\partial u^s}{\partial \nu}(y) - \frac{\partial \Phi(x,y)}{\partial \nu(y)} u^s(y) \right) ds(y), \quad x \in \mathbb{R}^m \setminus \overline{G}, \tag{7}$$

$$u^\infty(\hat{x}) = \gamma \int_{\partial G} \left(e^{-i\kappa \hat{x} \cdot y} \frac{\partial u^s}{\partial \nu}(y) - \frac{\partial e^{-i\kappa \hat{x} \cdot y}}{\partial \nu(y)} u^s(y) \right) ds(y), \quad \hat{x} \in \mathbb{S}, \tag{8}$$

with the constant

$$\gamma := \begin{cases} \dfrac{e^{i\pi/4}}{\sqrt{8\pi\kappa}}, & m = 2, \\ \dfrac{1}{4\pi}, & m = 3, \end{cases} \tag{9}$$

where (8) is known as *farfield representation*. In fact, the formula holds for every domain G for which u^s can be analytically extended into $\mathbb{R}^m \setminus G$. For the *single-layer* and *double-layer* potentials we use the notation

$$(\tilde{S}\varphi)(x) := \int_{\partial G} \Phi(x,y) \varphi(y) ds(y), \tag{10}$$

$$(\tilde{K}\varphi)(x) := \int_{\partial G} \frac{\partial \Phi(x,y)}{\partial \nu(y)} \varphi(y) ds(y), \tag{11}$$

for $x \in \mathbb{R}^m$. Green's formula for the field u^s in G can be written in the form

$$u^s = \tilde{S} \frac{\partial u^s}{\partial \nu} - \tilde{K} u^s \quad \text{in } G. \tag{12}$$

We also need the *boundary integral operators*

$$(S\varphi)(x) := 2 \int_{\partial G} \Phi(x,y) \varphi(y) ds(y), \tag{13}$$

$$(K\varphi)(x) := 2 \int_{\partial G} \frac{\partial \Phi(x,y)}{\partial \nu(y)} \varphi(y) ds(y), \tag{14}$$

for $x \in \partial G$.

It is well known that the combined single- and double-layer potential (first introduced by Brackhage-Werner, compare [3])

$$P\varphi := \tilde{K}\varphi - i\eta \tilde{S}\varphi \tag{15}$$

for the domain $G = D$ with continuous or L^2-density φ solves the scattering problem (3) - (5) if the density φ is a solution to the *boundary integral equation*

$$(I + K - i\eta S)\varphi = -2u^i. \tag{16}$$

The boundary integral equation has a unique solution in $C(\partial D)$. This approach works both for the case of one single scatterer D or when D consists of several separate components as shown in figure 1. We will use this approach for generation of our simulated far field patterns.

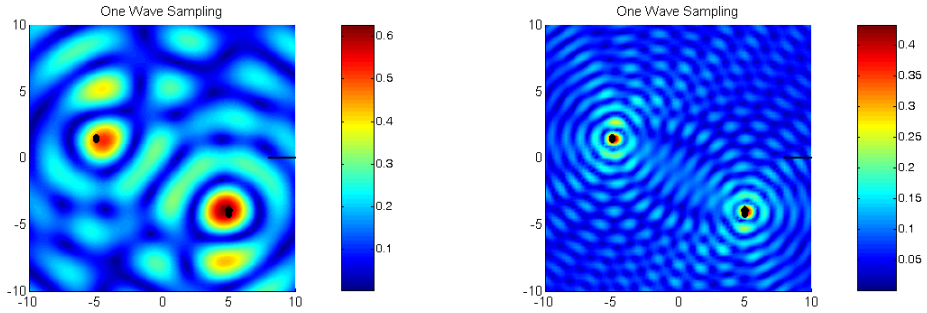

Figure 2: Behaviour of the functional $\mu(\tilde{y}, \kappa)$ for $\kappa = 1$ (left) and $\kappa = 3$ (right). The functional is the sum of two functionals of the form as shown in Figure 3. Here the approximate location of the two scatterers can clearly be detected. For low frequency the precision is not very high due to the superposition effects from the two point-spread functions of Figure 3.

For the analysis of the inverse problems, we will also work with a simpler representation of the scattered field by a single-layer potential. By Green's second theorem we obtain

$$0 = \int_{\partial D} \left(\Phi(x,y) \frac{\partial u^i}{\partial \nu}(y) - \frac{\partial \Phi(x,y)}{\partial \nu(y)} u^i(y) \right) ds(y), \tag{17}$$

for any $x \in \mathbb{R}^m \setminus \overline{D}$. Adding (7) and (17) we obtain

$$u^s(x) = \int_{\partial D} \Phi(x,y) \frac{\partial u}{\partial \nu}(y)\, ds(y), \quad x \in \mathbb{R}^m \setminus \overline{G}, \tag{18}$$

where we used $u(x) = u^i(x) + u^s(x) = 0$ for $x \in \partial D$ according to the Dirichlet boundary condition. This yields

$$u^\infty(\hat{x}) = \gamma \int_{\partial D} e^{-i\kappa \hat{x} \cdot y} \frac{\partial u}{\partial \nu}(y)\, ds(y), \quad \hat{x} \in \mathbb{S} \tag{19}$$

for the far field pattern with the constant γ given by (9).

3 One-wave fixed frequency sampling

We use equation (19) as a starting point to motivate a sampling scheme for one wave with fixed frequency. Assume that a scatterer D is of a size or smaller than the wavelength $\lambda = 2\pi/\kappa$. Let y_0 be a point in D, for example its geometric center. In this case we can approximate the far field pattern arising from D by

$$u^\infty(\hat{x}) = \gamma \int_{\partial D} e^{-i\kappa \hat{x} \cdot y} \frac{\partial u}{\partial \nu}(y)\, ds(y), \tag{20}$$

$$= \gamma e^{-i\kappa \hat{x} \cdot y_0} \int_{\partial D} e^{-i\kappa \hat{x} \cdot (y - y_0)} \frac{\partial u}{\partial \nu}(y)\, ds(y), \tag{21}$$

for $\hat{x} \in \mathbb{S}$. If $\kappa(y - y_0) \approx 0$ is small we can approximate the exponential term by $e^0 = 1$ and obtain

$$\begin{aligned} u^\infty(\hat{x}) &= \gamma e^{-i\kappa\hat{x}\cdot y_0} \int_{\partial D} \frac{\partial u}{\partial \nu}(y)\, ds(y), \\ &= C_D e^{-i\kappa\hat{x}\cdot y_0}, \quad \hat{x} \in \mathbb{S}, \end{aligned} \tag{22}$$

with

$$C_D = \gamma \int_{\partial D} \frac{\partial u}{\partial \nu}(y)\, ds(y). \tag{23}$$

The full far field pattern for scattering by multiple small scatterers

$$D = D_1 \cup ... \cup D_N \tag{24}$$

with centers $y_1, ..., y_N$ will be the sum

$$u^\infty(\hat{x}) = \sum_{j=1}^{N} C_{D_j} e^{-i\kappa\hat{x}\cdot y_j}, \quad \hat{x} \in \mathbb{S}. \tag{25}$$

We abbreviate $C_j := C_{D_j}$ for $j = 1, ..., N$. As a next step towards our sampling algorithm we multiply (25) by the factor

$$f(\hat{x}, \tilde{y}) := e^{i\kappa\hat{x}\cdot\tilde{y}}, \quad \hat{x} \in \mathbb{S}, \quad \tilde{y} \in \mathbb{R}^m \tag{26}$$

and integrate over $\mathbb{S}$. This yields

$$\begin{aligned} \mu(\tilde{y}, \kappa) &:= \Big| \int_{\mathbb{S}} e^{i\kappa\hat{x}\cdot\tilde{y}} u^\infty(\hat{x})\, ds(\hat{x}) \Big| \\ &= \Big| \sum_{j=1}^{N} C_j(\kappa) \int_{\mathbb{S}} e^{-i\kappa\hat{x}\cdot(y_j - \tilde{y})}\, ds(\hat{x}) \Big| \end{aligned} \tag{27}$$

for $\tilde{y} \in \mathbb{R}^m$ and $\kappa > 0$. The functional $\mu(\tilde{y}, \kappa)$ is the modulus of a linear combination

$$\mu(\tilde{y}, \kappa) = \Big| \sum_{j=1}^{N} C_j(\kappa)\, \mu_j(\tilde{y}, \kappa) \Big| \tag{28}$$

of the functionals

$$\mu_j(\tilde{y}, \kappa) := \int_{\mathbb{S}} e^{-i\kappa\hat{x}\cdot(y_j - \tilde{y})} ds(\hat{x}), \quad \tilde{y} \in \mathbb{R}^m. \tag{29}$$

Before we go into a deeper analysis of the behaviour of this functional we formulate the sampling algorithm for *one* fixed frequency and *one* time-harmonic wave.

ALGORITHM 3.1 (ONE-WAVE-FIXED-FREQUENCY ORTHOGONALITY SAMPLING) *For fixed wave number* κ orthogonality sampling *calculates*

$$\mu(\tilde{y},\kappa) = \left| \int_{\mathbb{S}} e^{i\kappa\hat{x}\cdot\tilde{y}} u^{\infty}(\hat{x})\, ds(\hat{x}) \right| \tag{30}$$

on a grid $\mathcal{G}$ *of points* $\tilde{y} \in \mathbb{R}^m$ *from the knowledge of the far field pattern* u^{∞} *on* $\mathbb{S}$. *Then, it searches the location of the unknown obstacles as the local maxima of the functional* $\mu(\cdot,\kappa)$.

Remark. The name *orthogonality sampling* has risen in discussions of the algorithm since the functional basically tests the orthogonality

$$\langle e^{i\kappa\hat{x}\cdot\tilde{y}}, u^{\infty}\rangle_{L^2(\mathbb{S})}, \quad \tilde{y} \in \mathbb{R}^m. \tag{31}$$

The multi-frequency case will be discussed in the following section.

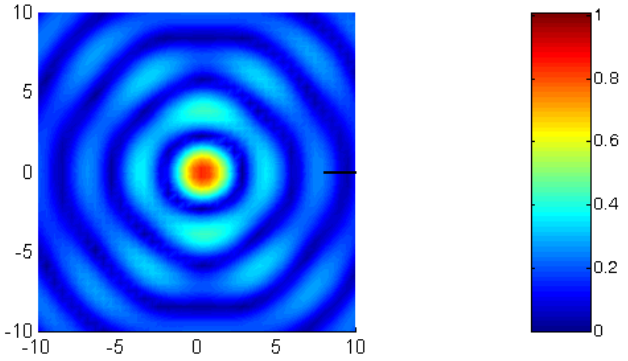

Figure 3: Behaviour of the functional $\mu_j(\tilde{y},\kappa)$ for $\kappa = 1$. The maximum is reached at the point $\tilde{y} = \tilde{y}_j$, here at the point $\tilde{y}_1 = (1,0)$ for $j = 1$. This function is also denoted as *point spread function* with center $\tilde{y}_1$.

For our analysis we first study the functional $\mu_j(\tilde{y},\kappa)$, $\tilde{y} \in \mathbb{R}^m$ defined by (29).

1. For $\tilde{y} = y_j$ we have $exp(i\kappa\hat{x}\cdot 0) = 1$ for all $\hat{x} \in \mathbb{S}$. This yields

$$\mu_j(\tilde{y}_j,\kappa) = \begin{cases} 2\pi & m = 2, \\ 4\pi & m = 3. \end{cases} \tag{32}$$

2. For the general case we can use the *Funk-Hecke Formula* [3]

$$\int_{\mathbb{S}} e^{-i\kappa z\cdot\hat{x}} Y_n(\hat{x})\, ds(\hat{x}) = \lambda_n j_n(\kappa r) Y_n(\hat{z}), \tag{33}$$

where $r = |z|$ with the spherical harmonics Y_n of order n, the spherical Bessel function j_n and

$$\lambda_n = \begin{cases} 2\pi & m = 2 \\ \frac{4\pi}{i^n} & m = 3 \end{cases} \tag{34}$$

A graph of the functional is shown in Figure 3. We are now prepared to formulate the following result for the mono-frequency case. We consider the following result as a first step towards a convergence analysis of the sampling method. It clarifies the identity of the indicator function.

THEOREM 3.2 (RECONSTRUCTION OF REDUCED SCATTERED FIELDS) *For scattering by an obstacle D with boundary ∂D by (31) we reconstruct the field*

$$u^s_{red}(\tilde{y}) := \gamma\lambda_n \int_{\partial D} j_0(\kappa|\tilde{y} - y|)\frac{\partial u(y)}{\partial \nu(y)} ds(y), \quad \tilde{y} \in \mathbb{R}^m. \tag{35}$$

Here we call the field (35) the reduced scattered field *for scattering by D. For scattering by N small scatterers with centers y_j, $j = 1, ..., n$ the* orthogonality sampling algorithm *(31) reconstructs the function*

$$u^s_{red}(\tilde{y}) := \gamma\lambda_n \sum_{j=1}^{N} C_j(\kappa) j_0(\kappa|\tilde{y} - y_j|), \quad \tilde{y} \in \mathbb{R}^m. \tag{36}$$

The expression (36) is an approximation for this reduced scattered field for small scatterers.

Proof. Consider the orthogonality sampling functional (31) applied to the far field pattern u^∞. We use the representations (25) or (19), respectively. Then, we employ the Funk-Hecke formula (33) applied to either (25) or (19) and exchange the order of integration to arrive at (36) or (35), respectively. □

The function reconstructed by the orthogonality sampling algorithm visualizes the location and shape of an object. Figure 2 shows a plot of this function for two small objects for wave number $\kappa = 1$ (left) and wave number $\kappa = 3$ (right). From the numerical results we clearly see that the maxima of the function can be used to locate the objects under consideration, in particular for the higher wave number $\kappa = 3$. The above result provides some insight into the role of the indicator function, but it is not a convergence proof. It is an *open problem* to analyse the relation between the reduced scattered field and the boundary of the unknown scatterer. Here, we will end this part of the analysis with a stability statement.

THEOREM 3.3 (STABILITY OF ORTHOGONALITY SAMPLING) *The reconstruction of the reduced scattered field u^s_{red} from the far field pattern u^∞ for scattering of a time-harmonic field u^i is linear and bounded from $L^2(\mathbb{S})$ into $BC(\mathbb{R}^m)$, $m = 2, 3$ with a norm given by the square root of the area of the unit circle or unit sphere, respectively.*

Proof. Clearly, the functional (31) is a linear mapping on $L^2(\mathbb{S})$. Denote the surface area of $\mathbb{S}$ by $|\mathbb{S}|$. Using the Cauchy-Schwarz inequality we estimate

$$\left|\left|\mu(\cdot,\kappa)\right|\right|_{BC(\mathbb{R}^m)} \leq |\mathbb{S}|^{1/2} \, ||u^\infty||_{L^2(\mathbb{S})}, \tag{37}$$

which yields the statement of the theorem. □

4 A one-wave multi-frequency sampling algorithm

The goal of this section is to extend the above sampling scheme to a multi-frequency situation. We will see that the results are significantly improved when several frequencies are taken into account.

We start with equation (19), where we now assume that $u^\infty = u^\infty(\hat{x},\kappa)$ depends on the wave number κ and is given for $\kappa_1, ..., \kappa_M$ with some $M \in \mathbb{N}$. We recall the definition

$$\mu(\tilde{y},\kappa) := \left| \int_{\mathbb{S}} e^{i\kappa\hat{x}\cdot\tilde{y}} u^\infty(\hat{x},\kappa) ds(\hat{x}) \right| \tag{38}$$

for one frequency. Now, we sum over all frequencies, i.e. we define our *multi-frequency functional* by

$$\mu[MF](\tilde{y}) := \int_{\mathbb{R}} \left| \int_{\mathbb{S}} e^{i\kappa\hat{x}\cdot\tilde{y}} u^\infty(\hat{x},\kappa) ds(\hat{x}) \right| d\kappa, \tag{39}$$

for $\tilde{y} \in \mathbb{R}^m$. Here, it is important to use the modulus in (39) *before* integrating the different frequencies. We have also tested to sum the reduced fields for different frequencies without taking the modulus and then study the modulus of the sum, which did *not* yield any reasonable reconstructions!

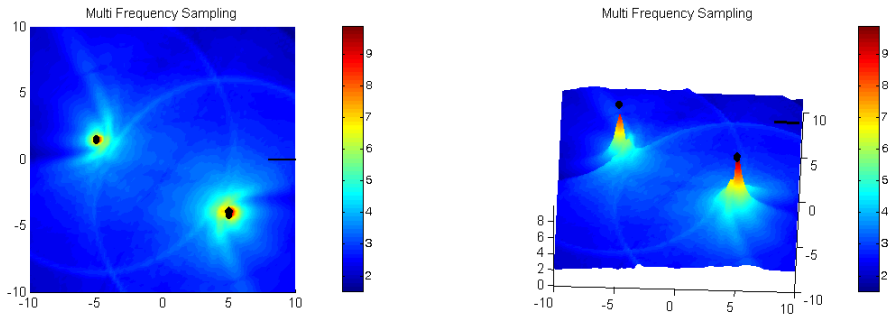

Figure 4: Behaviour of the multi-frequency functional $\mu[MF](\tilde{y})$ for two scatterers, where the incident wave is coming from the right-hand side. Here we used 20 equally distributed frequencies between $\kappa = 0.1$ and $\kappa = 6$.

For the particular situation for small obstacles from (25) we obtain the representation

$$\begin{aligned}\mu(\tilde{y}) &= \sum_{j=1}^{N} \int_{\mathbb{R}} C_j(\kappa) \Big| \int_{\mathbb{S}} e^{-i\kappa\hat{x}\cdot(y_j-\tilde{y})} ds(\hat{x}) \Big| \, d\kappa \\ &= \sum_{j=1}^{N} \int_{\mathbb{R}} C_j(\kappa)\mu_j(\tilde{y},\kappa) \, d\kappa \end{aligned} \tag{40}$$

Please note that this is *not* the Fourier transform of a function as it is usually employed for the Born approximation, where the dependency on the frequency and multiple scattering is neglected. A numerical study for the function (39) is carried out in Section 6.

5 The multi-direction multi-frequency setting

Finally, we have tested the sampling for one frequency and multiple incident directions as well as for the multi-direction multi-frequency case. The functionals for this are a generalization of the above one-wave single-frequency and one-wave multi-frequency cases. However, we would like to remark that it is very important for the visualization results where we take the modulus. We also tried to sum the functionals without taking the modulus of the reduced field, which did not yield any reasonable reconstructions. We define

$$\mu[MD](\tilde{y},\kappa) := \int_{\mathbb{S}} \Big| \int_{\mathbb{S}} e^{i\kappa\hat{x}\cdot\tilde{y}} u^{\infty}(\hat{x},\theta,\kappa) ds(\hat{x}) \Big| \, ds(\theta) \tag{41}$$

for $\tilde{y} \in \mathbb{R}^m$ and fixed $\kappa \in \mathbb{R}^+$ for the fixed frequency case and

$$\mu[MDMF](\tilde{y}) := \int_{\kappa_0}^{\kappa_1} \int_{\mathbb{S}} \Big| \int_{\mathbb{S}} e^{i\kappa\hat{x}\cdot\tilde{y}} u^{\infty}(\hat{x},\theta,\kappa) ds(\hat{x}) \Big| \, ds(\theta) d\kappa \tag{42}$$

as the functional for multi-direction multi-frequency (MDMF) sampling.

Remark. The above functionals are a generalized 'orthogonality' tests. We have tested several other settings, but there are many possible versions of the functionals to investigate and analyse. In this pilot paper we restrict our further task to showing numerical evidence that the above functionals are of large interest for shape reconstruction. So far the theoretical justification of the method for the multi-direction or multi-frequency case is open.

A numerical study for the indicator functions (41) and (42) is carried out in Section 6. We will show numerical evidence that the functional provides very good reconstructions of multiple scatterers with Dirichlet boundary condition if the range of frequencies and directions of incidence are chosen sufficiently large. Here, we note the stability of both functionals in the following theorem.

THEOREM 5.1 *The construction of the functionsls $\mu[MD]$ and $\mu[MDMF]$ of the orthogonality sampling method (41) and (42) for multiple incident directions or multiple*

frequencies from the far field pattern u^∞ for scattering of a time-harmonic field u^i is bounded from $L^2(\mathbb{S})$ into $BC(\mathbb{R}^m)$, $m = 2, 3$.

Proof. A proof is analogous to Theorem 3.3. □

6 Numerical Results

The task of this part is to describe the numerical realization of the methods. We first discuss the simulation of the far field pattern. Then, we will provide a numerical study of the above functionals which visualize the scatterers under consideration.

For the calculation of the far field patterns as well as for simulations of the reduced scattered field (35) we have used the Nyström method as described in Colton and Kress [3]. For multiple scatterers we have not implemented the split of the weak singularity in the integrals, but ignored the singularity. This leads to very flexible code, for which scattering by various objects can be easily implemented, though having low order convergence. An example for a simulated total field for scattering by eight separate scatterers which basically consist out of two groups is shown in Figure 1.

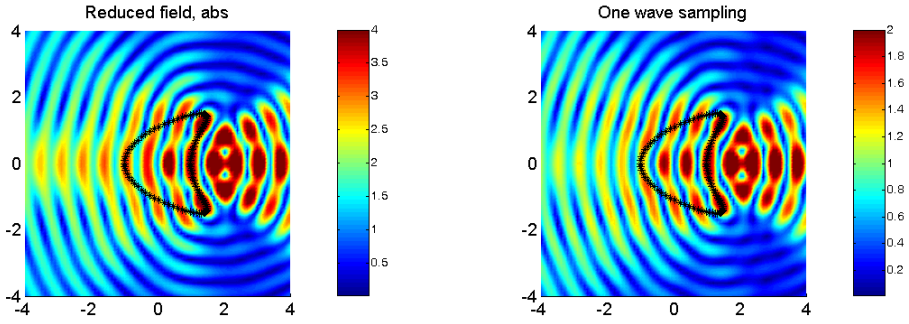

Figure 5: We compare the reduced field calculated via (35) with its reconstruction via orthogonality sampling (31). Here the wave number is $\kappa = 5$ and we consider a far field pattern for one plane wave with direction of incidence $d = (-1, 0)$. The true scatterer is indicated by the black dotted curve.

We have calculated the far field pattern in M equally distributed points

$$\hat{x}_j = j \cdot \frac{2\pi}{M}, \quad j = 0, ..., M-1, \tag{43}$$

via the discretized formula of the analogon to equation (8) for the Brackhage-Werner ansatz (15) with a density φ solving (16).

The combined potential (15) does not directly provide the normal derivative $\partial u/\partial \nu$. One can either calculate this normal derivative by appropriate boundary integral operators

or by solving a different more adequate integral equation. Here, we used the integral equation

$$S\frac{\partial u}{\partial \nu} = -u^i \tag{44}$$

on ∂D for the calculation of $\partial u/\partial \nu$, which is uniquely solvable for the case where the wave number κ is not an interior eigenvalue to the negative Laplacian. For our numerical simulations the numerical results with this approach have been quite satisfactory. The reduced field (35) could then been calculated by evaluation of the integral under consideration. A comparison between the reduced field calculated via (35) and its reconstruction via orthogonality sampling can be found in Figure 5.

We now show results for one-wave multi-frequency reconstructions via orthogonoality sampling. We will show results for some generic settings:

a) for several small scatterers

b) for a kite shaped scatterer

Results for the case a) of several small scatterers are shown in figures 4 and 6. The location of an unknown number of scatterers can be clearly seen in the graphics. It is an expected phenomenon that scatterers which are in the shadow of other scatterers cannot be seen when data for one direction of incidence only is used. In the two images of figure 6 we can find only the three out of 5 objects which are enlighted by the incoming plane wave, depending on the direction of incidence. The reconstruction of the shape of a kite is shown in figure 8. The method finds the enlighted side of the object very well. It does not find the shadow regions.

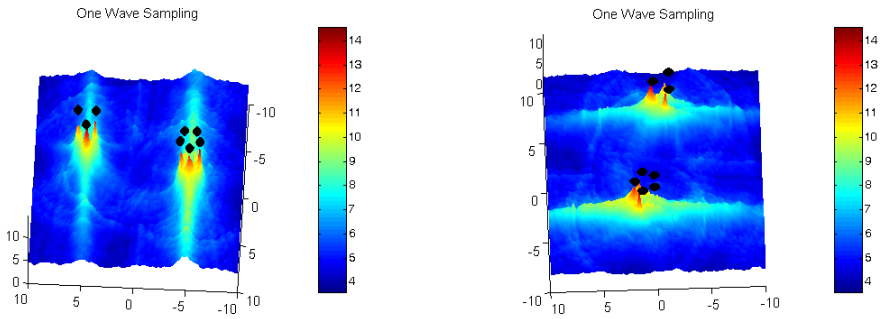

Figure 6: We show results of one-wave multi-frequency sampling, here with 20 wave numbers κ between $\kappa_0 = 0.1$ and $\kappa_1 = 10$. For the left image we used an incident wave with direction of incidence $d = (0, 1)$, for the right image we employed $d = (1, 0)$. The true scatterer is indicated by the black dotted curve.

Next, we would like to consider the fixed-frequency case where we use multiple directions of incidence. This case compares to the setting of the linear sampling method, the

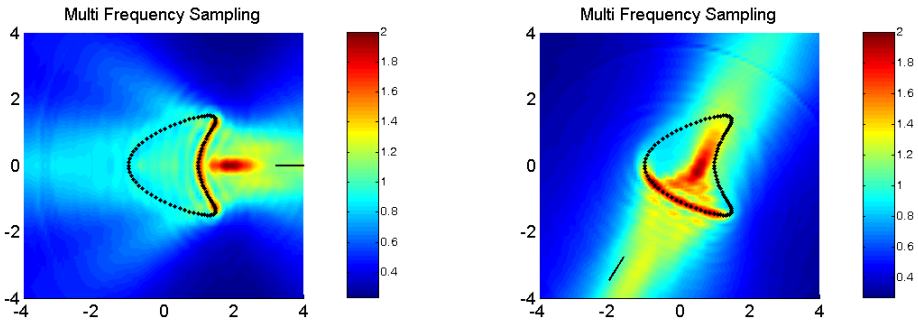

Figure 7: Now for the kite shaped scatterer we show results of one-wave multi-frequency sampling, here with 30 wave numbers κ between $\kappa_0 = 0.1$ and $\kappa_1 = 10$. The first image has been generated with direction of incidence $d = (-1, 0)$, the second with $d = (\cos(\pi/3), \sin(\pi/3))$. The true scatterer is indicated by the black dotted curve. The data include 2-3% stochastical error.

factorization method and the singular sources and probe methods. We will prove the the orthogonality sampling can generate images comparable to those of the linear sampling or factorization method, but with a well-posed sampling functional.

Finally, we show results for multi-direction multi-frequency (MDMF). We have generated far field data where several objects have been present. Then, we calculated the functional in a neighbourhood of each of the objects in a higher resolution, which is shown in figures 9, 10. This proves that detailed reconstruction of objects can be achieved even when other objects are present in space. In general, we have added 2-3% stochastical error to the data before carrying out the reconstructions.

References

[1] Colton, D. and Cakoni, F.: *Qualitative Methods in Inverse Scattering Theory* Springer, Series on Interaction of Mathematics and Mechanics (2006).

[2] Colton, D. and Kress, R.: *Integral equation methods in scattering theory.* John Wiley & Sons Inc. 1983.

[3] Colton, D. and Kress, R.: *Inverse Acoustic and Electromagnetic Scattering Theory.* Springer 1998, 2nd edition.

[4] Engl, H.W., Hanke, M. and Neubauer, A.: *Regularization of inverse problems*, Kluwer 1996.

[5] Kirsch, A. and Grinberg, N.: *The Factorization Method for Inverse Problems* Oxford Lecture Series in Mathematics & Its Applications No. 36 2008.

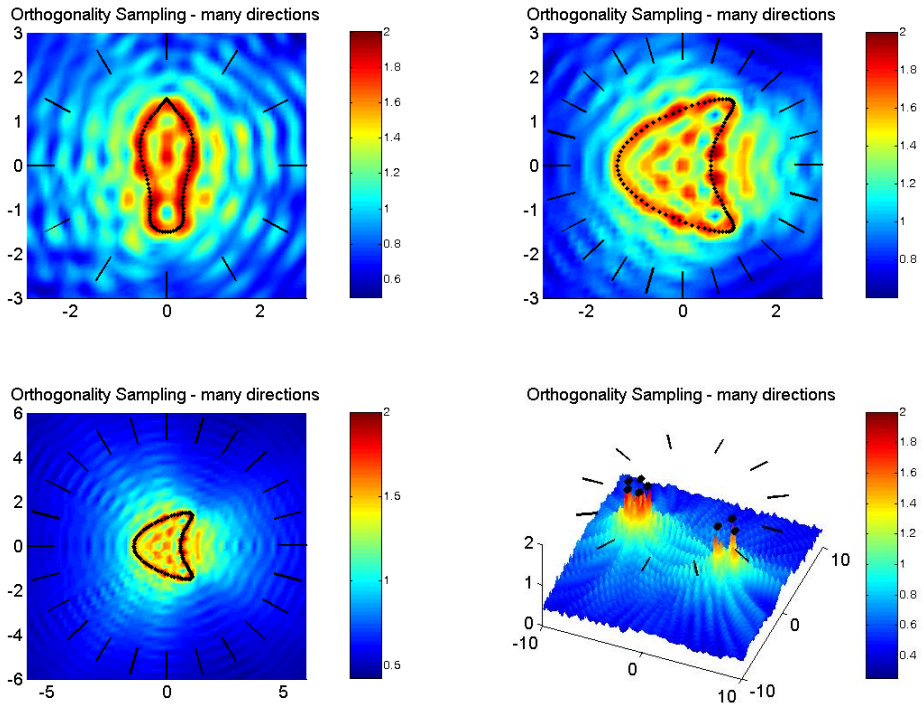

Figure 8: We show orthogonality sampling for 12 directions of incidence. Here we measure the far field pattern at 120 directions and one fixed wave number $\kappa = 6$. Similar images have been achieved already with 40 far field directions. The true scatterer is indicated by the black dotted curve. The data include 2-3% stochastical error.

[6] Kress, R.: Linear Integral Equations. Springer 1989.

[7] Kusiak, S., Potthast, R. and Sylvester, R.: "A 'range test' for determining scatterers with unknown physical properties." Inverse Problems 19, 533-547 (2003).

[8] Lax, P. and Phillips, R.S.: *Scattering Theory*, Academic Press (1967)

[9] Potthast, R.: A survey about sampling and probe methods for inverse problems. Topical Review. Inverse Problems 22 (2006), R1-47.

[10] Potthast. R.: *Point-sources and Multipoles in Inverse Scattering*, Chapman & Hall, London (2001).

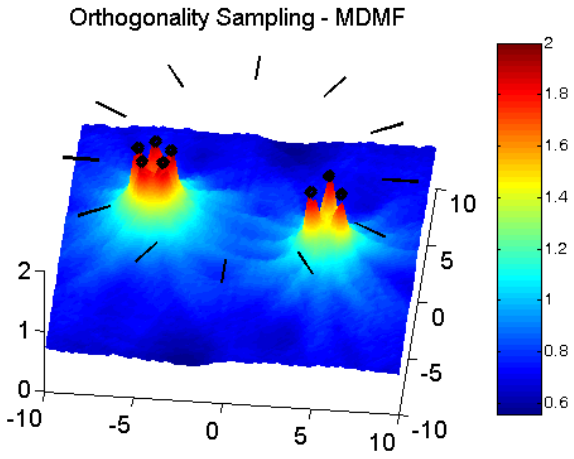

Figure 9: For multi-direction multi-frequency we show results of the orthogonality sampling functional for the scatterer with eight separate components. The data include 2-3% stochastical error.

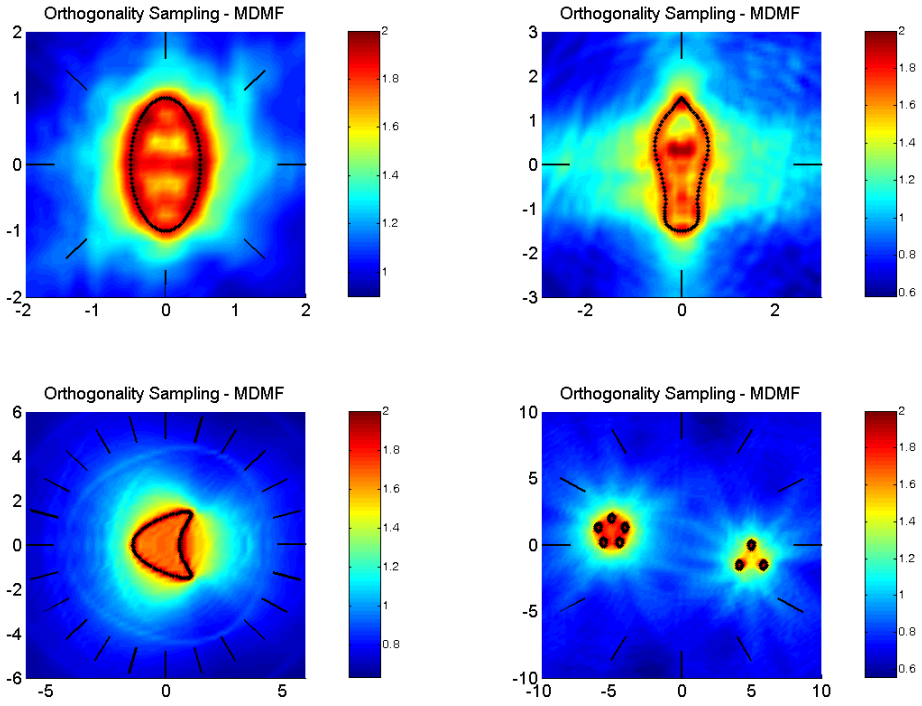

Figure 10: For multi-direction multi-frequency we show results of the orthogonality sampling functional. The reconstructions for the shape of the different scatterers have been cut out of larger images, where several scatterers have been included. The true scatterer is indicated by the black dotted curve. The data include 2-3% stochastical error.